CROATICA CHEMICA ACTA CCACAA **64** (2) 139–152 (1991)

YU ISSN 0011-1643
UDC 546+541.1
CCA-1986

Original Scientific Paper

The Influence of Manganese and Silicon on Some Physicochemical Properties of Aluminophosphates Having the Sodalite Structure

Jurka Batista[1], *Venčeslav Kaučič*[1,2], *and Stanko Hočevar*[1]

[1]*Boris Kidrič Institute of Chemistry, P.O. Box 30, 61115 Ljubljana, Slovenia (YU)*
[2]*Department of Chemistry and Chemical Technology, University of Ljubljana, 61000 Ljubljana, Slovenia (YU)*

Received October 29, 1990

Aluminophosphate and silicoaluminophosphate materials of the sodalite structure type with manganese have been synthesized. A comparative study of $AlPO_4$-20, $AlPO_4$-20(Mn), SAPO-20, and SAPO-20(Mn) properties has been carried out by using the X-ray powder diffraction analysis, SEM, qualitative EDAX-micro analysis, chemical and thermal analysis, IR, EPR and diffuse reflectance spectroscopy. Chemical modification of $AlPO_4$-20 with manganese and silicon leads to changes in the cubic unit cell parameters and in the thermal properties. The EPR and DRS data for as-synthesized $AlPO_4$-20(Mn) and SAPO-20(Mn) materials show the presence of octahedrally coordinated non-framework Mn, while the unit cell parameter data and the thermal behaviour of the samples are not so conclusive regarding the location of Mn.

INTRODUCTION

Crystalline, microporous aluminophosphates ($AlPO_4$-n)[1] and $AlPO_4$-based molecular sieves with one or more additional elements incorporated into the framework[2,3] are very interesting materials because of their catalytic and adsorptive properties and also because of the remarkable diversity in their crystal structures. Incorporation of additional elements into the $AlPO_4$ framework led to the discovery of new structures and gave new possibilities of controlling the catalytic and adsorptive properties of these materials. Synthesis and characterization of the named materials have been extensively investigated. However, the number of papers on this theme is still increasing.

Aluminophosphate-based materials having the sodalite structure[4] have been synthesized with tetramethylammonium hydroxide template.[1-6] The synthesis, the influence of manganese and silicon on the physicochemical properties of aluminophosphates with the sodalite structure and the Mn coordination are presented in this work.

EXPERIMENTAL

Reagents

Silica sol (30% Tosil, Neštemice) was of a technical grade. H_3PO_4 (85%, Kemika-Zagreb), manganese(II) acetate (Kemika-Zagreb), manganese(II) sulfate (Merck) and aluminium isopropoxide (98%. Aldrich) were pro analysi. Tetramethylammonium hydroxide (25%, Fluka) was of a practical grade. Pseudoboehmite (69.4% Al_2O_3) was prepared according to reference 8.

Instrumentation

The X-ray powder diffraction analysis was carried out on a Philips PW 1710 diffractometer with CuKα radiation and in the range 2ϑ of 4–70 °. The unit cell constant of the synthesized materials was determined with α-quartz IMSIL-A-25, 1.1 μm (99.5±0.5% SiO_2, Illinois Mineral Co., U.S.A.) as internal standard at the scanning rate 0.24 ° 2ϑ min^{-1}. Thermal analysis was performed in air using thermal analyser (Mettler 2000C model) under the following experimental conditions: flow of dry air 2.1 l h^{-1}, reference compound α-Al_2O_3, sample holder platinum crucible, temperature range 25–1000 °C, heating rate 10 °min^{-1}. For some samples, the thermal analysis was repeated in static air atmosphere on a Du Pont 2000 instrument. IR spectra were recorded on a FTIR Digilab-FTS-80-type spectrophotometer in the 4000–400 cm^{-1} region with KBr pellets. Diffuse reflectance spectra were obtained on a Varian DMS 80 UV-VIS spectrophotometer in the 750–200 nm range, with teflon as standard. EPR spectra were measured on a Varian E-9, 9.3 GHz instrument (scan range 400 mT, field set 330 mT, modulation amplitude 0.4 mT, microwave power 40mW and gain: 20, 200 and 400). Varian »Strong Pitch« was used as standard to determine the concentration of paramagnetic centres. Polycrystalline radical diphenyl-picrylhydrazyl was used to determine *g*-values. Characterization of the spectra was made by a computer program for variation of the broadness of individual hyperfine components. EDAX (energy dispersive analysis by X-ray) microprobe analysis in conjunction with SEM was taken on clear crystals from products with LEITZ AMR-1600 T apparatus.

Quantitative chemical analysis (Si, Al, P were determined photometrically, and Mn by atomic absorption spectroscopy) gave overall product compositions listed in Table II.

The SEM micrographs of samples were obtained with a JEOL JSM-T 220 apparatus.

Synthesis

SAPO-20 and SAPO-20(Mn) samples were synthesized according to procedures described in Union Carbide patents.[2,7] $AlPO_4$-20 synthesis was based on the description given in example 47 of the Union Carbide patent[1] and also on information from the literature.[6] A similar procedure was used for $AlPO_4$-20 modified with manganese. Detailed experimental data are given in Table I. Hydrothermal crystallization from reactive gels was carried out in stainless-steel teflon-lined laboratory autoclaves (volume 50 cm^3), without stirring, varying the time (1–5 days) and temperature (125–195 °C) of crystallization. Washed and dried samples were calcined in air at 500 °C for one hour.

RESULTS AND DISCUSSION

X-ray powder diffraction patterns of as-synthesized materials indicate that the materials possess the sodalite structure.[4] Crystalline and phase pure samples have been analyzed. SAPO-20 materials attain the highest crystallinity. Similar materials which contain manganese (designated as SAPO-20(Mn)) attain about 45% of the SAPO-20 crystallinity. The lowest crystallinity (about 25% of the SAPO-20) is characteristic for $AlPO_4$-20 and $AlPO_4$-20(Mn) materials. (The method used to obtain the degree of crystallinity is based on the sum of the intensities of ten strongest reflections).

Chemical composition of the selected materials is listed in Table II. It is evident that the Si content in the SAPO-20 materials increases with increasing the Si content

TABLE I

Synthesis conditions

Sample No.	Type of product	Gel composition (molar oxide ratios)* $(TMAOH)_m:(Al_xP_ySi_zMn_w)O_2:(H_2O)_n$						Crystallization	
		m	x	y	z	w	n	*T* °C	Time
1[a,c]	$AlPO_4$-20	0.25	0.50	0.50	0	0	12.5	160	40 h
2[b,d,e]	$AlPO_4$-20(Mn)	0.25	0.40	0.50	0	0.100	12.5	195	7 d
3[a,c,e]	$AlPO_4$-20(Mn)	0.24	0.48	0.48	0	0.048	11.9	160	40 h
4[a]	SAPO-20	0.50	0.40	0.40	0.20	0	12.0	160	9 d
5[a]	SAPO-20	0.30	0.40	0.40	0.20	0	10.0	160	3 d
6[a]	SAPO-20	0.30	0.30	0.30	0.40	0	10.0	160	3 d
7[a]	SAPO-20	0.30	0.20	0.20	0.60	0	10.0	160	3 d
8[a]	SAPO-20(Mn)	0.23	0.41	0,41	0.14	0.045	11.4	195	5 d
9[b]	SAPO-20(Mn)	0.23	0.20	0.35	0.37	0.075	11.4	195	5 d
10[b]	SAPO-20(Mn)	0.23	0.30	0.40	0.25	0.050	11.4	195	5 d

* Al_2O_3 source was pseudoboehmite (a) and aluminium isopropoxide (b), x+y+z+w = 1.
[c] Gel was previously aged at 0 °C for 2 days.
[d] $AlPO_4$-20(Mn) contains impurity ($AlPO_4$-berlinite).[9]
[e] $MnSO_4$ was used instead of Mn(II)-acetate.

TABLE II

Chemical composition of the as-synthesized samples

Sample No.	Oxide composition	H_2O content[a]	Organic content[a]	Approx. molecules/cage[a]	
		(g/g)	(g/g)	H_2O	TMA
1	$(Al_{0.55}P_{0.45})O_2$	0.078	0.127	2.0	0.8
3	$(Al_{0.47}P_{0.49}Mn_{0.04})O_2$	0 059	0.085	1.4	0.5
4	$(Si_{0.18}Al_{0.48}P_{0.34})O_2$	0.023	0.080	0.5	0.4
5	$(Si_{0.17}Al_{0.50}P_{0.33})O_2$	0.024	0.143	0.6	0.8
6	$(Si_{0.27}Al_{0.42}P_{0.31})O_2$	0.036	0.080	0.8	0.4
7	$(Si_{0.23}Al_{0.50}P_{0.27})O_2$	0.018	0.100	0.4	0.5
8	$(Si_{0.13}Al_{0.42}P_{0.40}Mn_{0.04})O_2$	0.047	0.078	1.1	0.4
9	$(Si_{0.41}Al_{0.19}P_{0.32}Mn_{0.08})O_2$	0.030	0.078	0.7	0.4
10	$(Si_{0.28}Al_{0.30}O_{0.37}Mn_{0.05})O_2$	0.015	0.150	0.4	0.9

[a] From TGA and DSC

in the synthesis mixture (Table I, samples 5–7). On the other hand, the Si content in SAPO-20 in sample 7 is only 0.23, although this value is 0.60 in the gel. The pH value of the synthesis gel is between 8.2–8.5. Further comparison of the Si content in SAPO-20 (sample 4) and SAPO-20 (sample 5) prepared from gels with different TMAOH concentrations (pH = 8.2–9.4 and pH = 6.0–7.2, respectively) suggests that there is a relationship between the TMAOH concentration in the reaction mixture and the amount of Si in the SAPO-20 materials. The higher content of Si in SAPO-20 (sample 4) can be explained by a better solubility of SiO_2 in alkaline reaction medium and by the influence of a higher TMA concentration on the connection of SiO_2 tetrahedra.[10] It seems that a too low ($TMAOH/SiO_2$) ratio in the gel (Table I, sample 7) limits the solubility of SiO_2 and this could be the reason why SAPO-20 with the highest Si-atom fraction can be prepared according to the synthesis conditions for sample 6 (x=y=0.30, z=0.40, m/z=0.75 and pH between 7.0–7.8).

Compositions of the synthesized SAPO-20 materials suggest possible isomorphous substitution mechanisms (SM). The theoretically possible SM in SAPO-n materials are:[2,11] SM1 (Si→Al), SM2 (Si→P) and SM3 (2Si→Al+P). The predominant one appears to be SM2, but SM3 may also appear. The nature of the SM and the extent of Si incorporation depend on the synthesis conditions. It seems that in SAPO-5 synthesis, the pH of the system determines which of the SM2 (at low Si) or (SM3+SM2) prevail.[11] A thorough study of three SAPO-20 materials has been done to investigate the mechanisms of Si substitution into the hypothetical aluminophosphate framework.[6] In two SAPO-20 samples (SM2+SM3) has been proved. In spite of ^{13}C, ^{29}Si, ^{27}Al and ^{31}P NMR studies, the SM in one of SAPO-20 materials still remains unclear. The chemical composition of our synthesized SAPO-20 materials (Table II) suggests also SM2 because in all cases the T-atom fraction of Al is higher than that of P. Only the composition of SAPO-20 (sample 6) suggests also SM3, since T-atom fractions of Al and P are both lower than 0.50. It is interesting that (SM2+SM3) seems to appear in the sample with the highest T-atom fraction of Si. (It is known that the contribution of SM3 seems to be possible only under specific synthesis conditions and leads to a certain Si loading[11]).

To obtain the unit cell parameters of as-synthesized and calcined samples, the XRD data were analyzed by the TREOR[12] and PARAM[13] programs. A cubic unit cell for as-synthesized $AlPO_4$-20, $AlPO_4$-20(Mn), SAPO-20, and SAPO-20(Mn) is given (Table III). Comparison of the unit cell parameters with those reported for $AlPO_4$-20 ($a_o = 8.933$ Å), and SAPO-20 ($a_o = 8.958$ Å)[14] leads to the conclusion that the presence of Mn and Si slightly expands the unit cell although the symmetry of the system does not change. The cubic symmetry of the sodalite structure is retained even after calcination, except in samples 7 and 9. The large change in the unit cell volume for the SAPO-20(Mn) materials can be explained by taking into account EPR and DRS measurements (see Table IV and V). These data show the presence of octahedrally coordinated manganese atoms which are probably located in the pores and the presence of these Mn-entities can be the reason for the relatively large change in the unit cell volume.

Figures 1, 2 and 3 show the TGA, DTG and DSC results, respectively, for aluminophosphate gel, $AlPO_4$-20, $AlPO_4$-20(Mn), SAPO-20, and SAPO-20(Mn). Differences in the thermal behaviour of these samples are substantial. Weight losses of water (25–

TABLE III

Unit cell parameters and unit cell volumes of as-synthesized samples: $AlPO_4$-20, $AlPO_4$-20(Mn), SAPO-20, and SAPO-20(Mn)

Sample No.	Type of product	As-synthesized	
		a(Å)	V (Å^3)
1	$AlPO_4$-20	8.9397 (8)	714.5 (2)
3	$AlPO_4$-20(Mn)	8.969 (1)	721.4 (3)
4	SAPO-20	9.0325 (3)	736.91 (8)
5	SAPO-20	9.0062 (2)	730.52 (6)
6	SAPO-20	9.0251 (3)	735.11 (7)
7	SAPO-20	9.0358 (2)	737.74 (6)
8	SAPO-20(Mn)	8.9945 (7)	727.7 (2)
9	SAPO-20(Mn)	9.0807 (3)	748.80 (7)
10	SAPO-20(Mn)	9.028 (2)	735.8 (4)

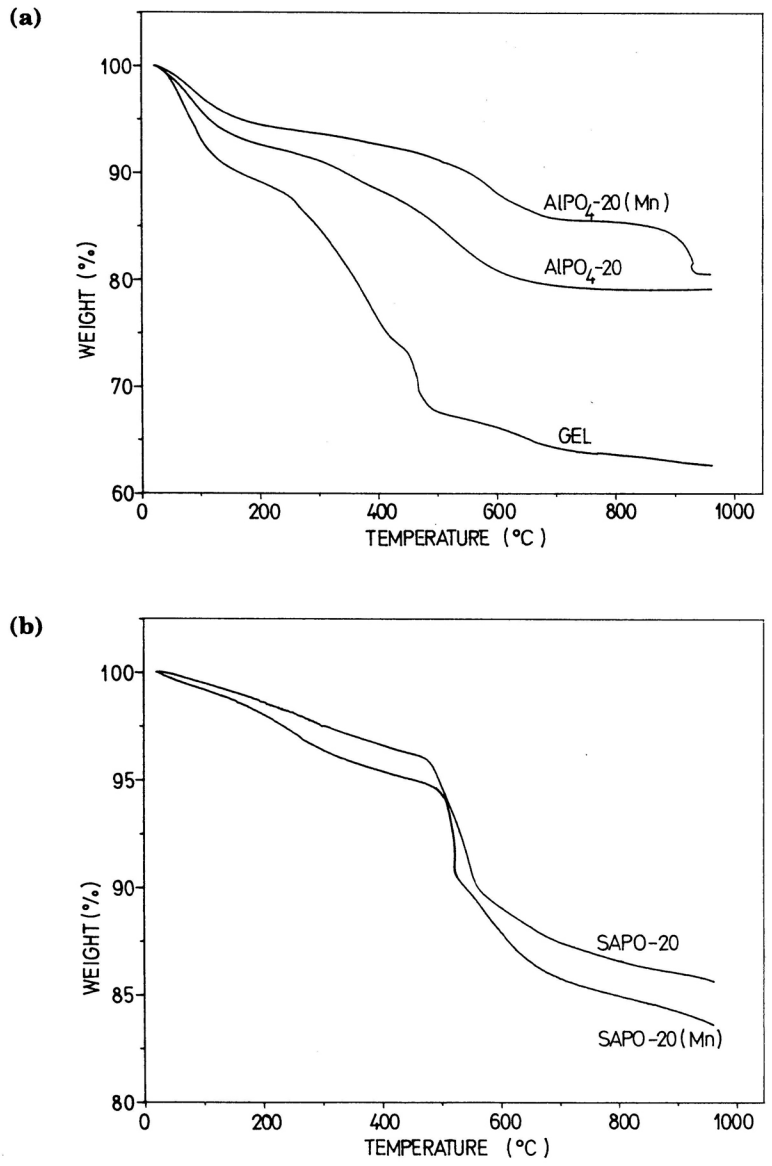

Figure 1. Thermogravimetric analyses: (a) aluminophosphate gel, $AlPO_4$-20, $AlPO_4$-20(Mn) and (b) SAPO-20 (sample 5), SAPO-20(Mn) (sample 8).

200 °C) and template (350–700 °C) in the gel are about twice as high as in $AlPO_4$-20 and $AlPO_4$-20(Mn) samples. The DTG and DSC curves correspond in shape and position of peaks for all three samples, indicating that there are no phase transitions present in the temperature interval between 25 and 700 °C. The DTG and DSC curves

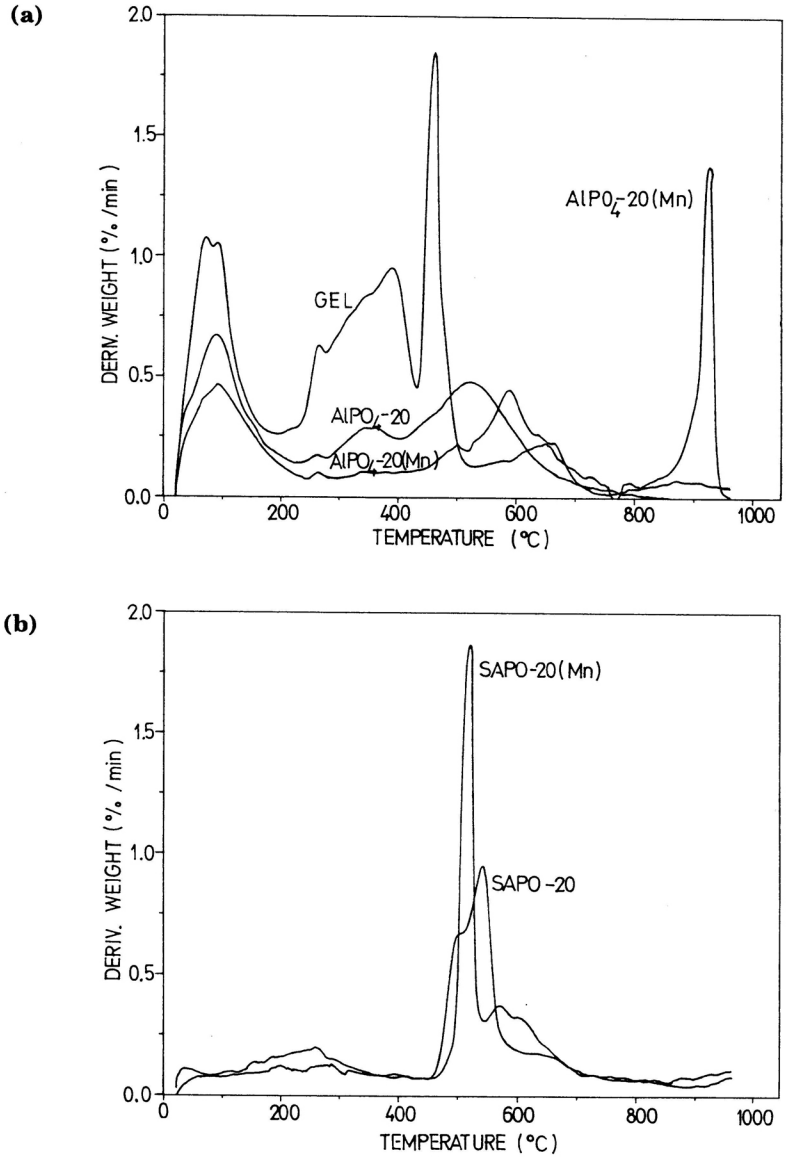

Figure 2. Differential thermogravimetric analyses: (a) aluminophosphate gel, $AlPO_4$-20, $AlPO_4$-20(Mn) and (b) SAPO-20 (sample 5), SAPO-20(Mn) (sample 8).

for the gel sample show two distinct peaks (DSC-endotherms) due to water loss at about 80 °C and 110 °C, a small peak (DSC-endotherm) at about 280 °C, and four successive peaks (DSC-exotherms) at about 410 °C, 460 °C, 480 °C and 610 °C due to oxidative decomposition of TMA. The peak at 460 °C is sharp and strong, the other peaks are

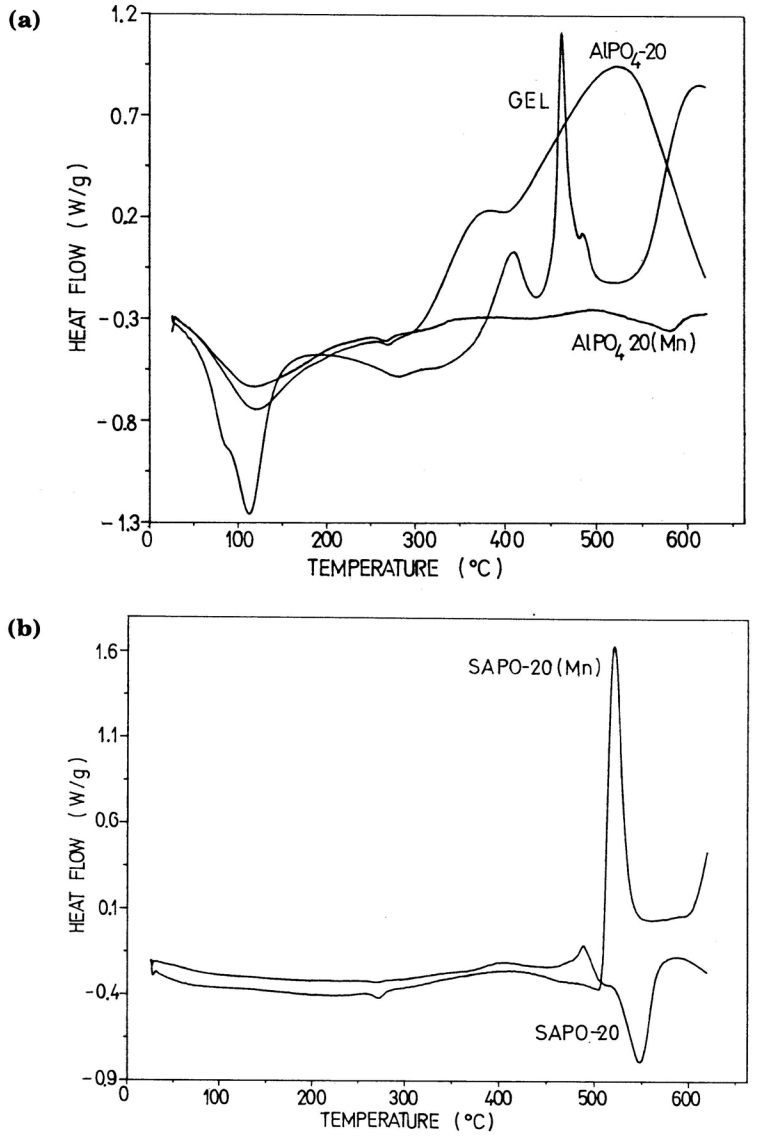

Figure 3. Differential scanning calorimetric analyses: (a) aluminophosphate gel, $AlPO_4$-20, $AlPO_4$-20(Mn) and (b) SAPO-20 (sample 5), SAPO-20(Mn) (sample 8).

more broadened. The TG and DSC curves of $AlPO_4$-20 have a single broad peak (DSC--endotherm) at about 120 °C due to water loss, a small peak (DSC-endotherm) at about 265 °C and successively two broad peaks (DSC-exotherms) at about 370 °C and 520 °C, indicating that the decomposition of TMA in $AlPO_4$-20 sample begins at a lower tem-

perature than in the gel sample. Also, decomposition steps of TMA are less distinct in $AlPO_4$-20 than in gel. DTG and DSC curves for $AlPO_4$-20(Mn) sample resemble those for AlPO-20, except that there is an additional DTG peak with the onset at about 850 °C belonging to decomposition of possibly occluded $MnSO_4$. The DSC water loss peak at about 120 °C and the two TMA decomposition peaks at about 365 °C and 500 °C have much lower intensities than for the $AlPO_4$-20 sample. There is also a medium strong endotherm present, with a peak at about 570 °C that belongs to the decomposition of TMA. This peak can be ascribed to the endothermal coke-forming reactions of hydrocarbon entities, formed in the first stage of decomposition of TMA, on the acidic centres present due to Mn incorporation into the framework of $AlPO_4$-20. The TG weight losses in the temperature interval 25–950 °C for $AlPO_4$-20 and $AlPO_4$-20(Mn) are comparable (20.85 wt% and 19.44 wt%, respectively). The $AlPO_4$-20 sample was white after the thermal analysis, while the $AlPO_4$-20(Mn) sample became dark due to coke deposition. It is interesting to follow the thermal behaviour of SAPO-20 and SAPO-20(Mn) samples. The weight loss of SAPO-20 can be divided into three stages. The first stage in the temperature interval between 25 °C and about 430 °C belongs to gradual loss of water. DTG curve shows a broad low-intensity peak at about 280 °C and the DSC curve also shows a broad low-intensity peak at about 270 °C. The second and the third stages belong to the decomposition of TMA in the temperature interval between 460 °C and 710 °C. DTG curve shows a relatively narrow strong-intensity two-peak range between 460 °C and 590 °C, with peaks located at about 510 °C and 570 °C and a broad low-intensity peak range between 590 °C and 710 °C with the peak located at about 620 °C. The DSC curve shows a low-intensity medium broad endotherm at about 450 °C that continues into the low-intensity sharp exotherm at about 500 °C. This exotherm is not fully developed since it is overhelmed by a strong and sharp endotherm at about 545 °C. Like for $AlPO_4$-20(Mn), it can be stated that this endotherm belongs to the coke-forming reactions of hydrocarbon species, formed during the decomposition of TMA, on the acidic centres formed due to the Si incorporated in the framework. The sample was black after thermal analysis. For SAPO-20 samples, the number and the temperature range of thermal effects depend on the oxide composition of the sample. Sample 7 exhibits the lowest thermal stability. The thermal decomposition of TMA and the gradual decomposition of the sodalite structure to amorphous material are simultaneous processes. The SAPO-20(Mn) TG curve shows a water loss region between 25 °C and 450 °C, and again the subsequent two-stage region belonging to TMA decomposition in the temperature interval between 470 °C and 710 °C. DTG curve shows a broad low-intensity peak at about 270 °C due to water loss and the same can be said for the DSC curve, which has a broad low-intensity endotherm at about 270 °C. DTG curve in the region of TMA decomposition shows a very sharp and strong peak at about 520 °C and a broad low-intensity peak at about 580 °C. The DSC curve shows also a strong and sharp exotherm at about 520 °C and the onset of a second exotherm at about 610 °C. There are no endotherms present in the temperature interval of TMA decomposition. Since the change of colour after the thermal analysis was not so drastic as for SAPO-20 sample, one can conclude that there are less strong acidic centres present in the SAPO-20(Mn) sample than in the SAPO-20 sample. Since both samples contain a considerable amount of Si incorporated into the framework, it can be concluded that Mn in SAPO-20(Mn) is not incorporated into the framework but rather forms Mn-entities in the cages that block the acidic centres of SAPO-20 due to Si incorporation into the framework. However, the data are not conclusive enough to state that none of the Mn is incorporated into the framework of SAPO-20(Mn). Only in

sample 10, the additional exothermal effect with accompanying weight loss appears in the temperature interval 240–285 °C. It can be ascribed to the decomposition of acetate in air atmosphere due to occluded manganese acetate species. It is interesting to note that sample 9 with the highest content of Si and Mn has the lowest thermal stability, which is confirmed also by the XRD analysis of the sample after thermal analysis. Powder diffractograms of materials calcined at 600 °C show a considerable degradation (samples 4–6) and/or appearance of a dense phase[9] (samples 3, 8, 10). The crystal structure is retained only in $AlPO_4$-20. From the weight loss due to water desorption and TMA decomposition, the approximate number of water and TMA molecules per sodalite cage was calculated (Table II). The calculation was based on the TO_2 concept,[15] and the fact that sodalite ideally gives one TMA per cage.[6,16]

Our observation about the position of the IR bands in the structural region (400–1400 cm^{-1}) for $AlPO_4$-20 (1136, 1105 cm^{-1}) and SAPO-20 (1111, 1060 cm^{-1}, sample 4) materials is in agreement with literature data.[6] The broad IR band in the region 1000–1100 cm^{-1} is characteristic of zeolite materials[17] and has been assigned to the asymmetric stretching of tetrahedra (ν_{as}). In $AlPO_4$-20 and SAPO-20, the position of ν_{as} band is shifted to a higher wavenumber because of the changes in the mean T–O bond.[15] A similar conclusion is valid for $AlPO_4$-20(Mn) (1146, 1078 cm^{-1}) and SAPO-20(Mn) (1111 cm^{-1}). The characteristic peak at 951–957 cm^{-1}, which may be attributed to C–N band in the quarternary ammonium compounds (TMAOH),[18] appeared in all synthesized materials.

On scanning electron micrographs of the as-synthesized samples (Figure 4), spherulites prevail. In $AlPO_4$-20 polycrystalline aggregates of spherules (1 μm) were obtained. SEM of $AlPO_4$-20(Mn) show spherulites (3–6 μm) and intergrowths of crystals. $AlPO_4$-20 and $AlPO_4$-20(Mn) materials have been prepared from gels which were aged prior to the crystallization (known method for preparing $AlPO_4$-20 without impurity[6]). Aging of the gels at low temperature before crystallization is a method that possibly leads to a decrease of the final crystal size, because crystal growth is prevented and a large number of nuclei is formed.[19] The uniformly shaped spherulites (15 μm) are in SAPO-20(Mn), sample 8.

In the EPR spectra of manganese in as-synthesized $AlPO_4$-20(Mn) and SAPO-20(Mn), the hyperfine structure is not evident,[20] which was ascribed to the locally high manganese concentration.[21] $AlPO_4$-20(Mn), SAPO-20(Mn) and gels with very low contents of Mn (0.001 wt%) were prepared instead (Table IV). In their EPR spectra, there are six resolved hyperfine lines with a mean distance of about 9.3 mT (Figure 5), corresponding to octahedral[22-25] Mn^{2+}. The comparison of our results with the MnAPO-5 EPR measurements[25] confirms the existence of octahedral non-framework manganese as well. After the calcination of the samples, the EPR spectra show the prevailing carbon radical, which hinders EPR comparative study of as-synthesized and calcined $AlPO_4$-20(Mn) and SAPO-20(Mn).

The diffuse reflectance spectra (Figure 6) of the as-synthesized samples and reference manganese compounds show several bands (Table IV). The band intensities of tetrahedral Mn^{2+} in the prepared $[(C_2H_5)_4N]_2MnCl_4$[25] are higher than the intensities of octahedral Mn^{2+} in $MnCl_2.4H_2O$ and this is in agreement with the literature data.[27,28] The observed band intensities and positions in the DR spectra of $AlPO_4$-20(Mn) and SAPO-20(Mn) show the presence of octahedrally coordinated manganese. The narrowest band is at 406 nm.

TABLE IV

Concentration of paramagnetic centres in prepared samples[20]

Samp. No.	Description	C (mol/cm^3)	EPR spectra
11	amorphous gel: TMAOH-Al_2O_3-P_2O_5-50H_2O	0	1)
12	mixture of amorphous gel + $MnSO_4.H_2O$	1.4. 10^{-7}	2)
13	mixture of amorphous gel + $MnSO_4.H_2O$	8.6. 10^{-8}	2)
6	SAPO-20	0	1)
6b	SAPO-20, impregnated with soln. of $MnSO_4$	3.7. 10^{-7}	4)
6c	SAPO-20, calcined and impregnated with soln. of $MnSO_4$	not determined	3)
3a	$AlPO_4$-20(Mn)	5.0. 10^{-8}	4)
8a	SAPO-20(Mn)	1.6. 10^{-7}	4)
11a	aluminophosphate gel containing Mn	5.4. 10^{-8}	4)

1) The sample contains impurity (»free« Fe^{3+} ion)
2) Without hyperfine structure.
3) Carbon radical 10^{-8} mol/cm^3.
4) Octahedrally coordinated non-framework Mn.[22-25]

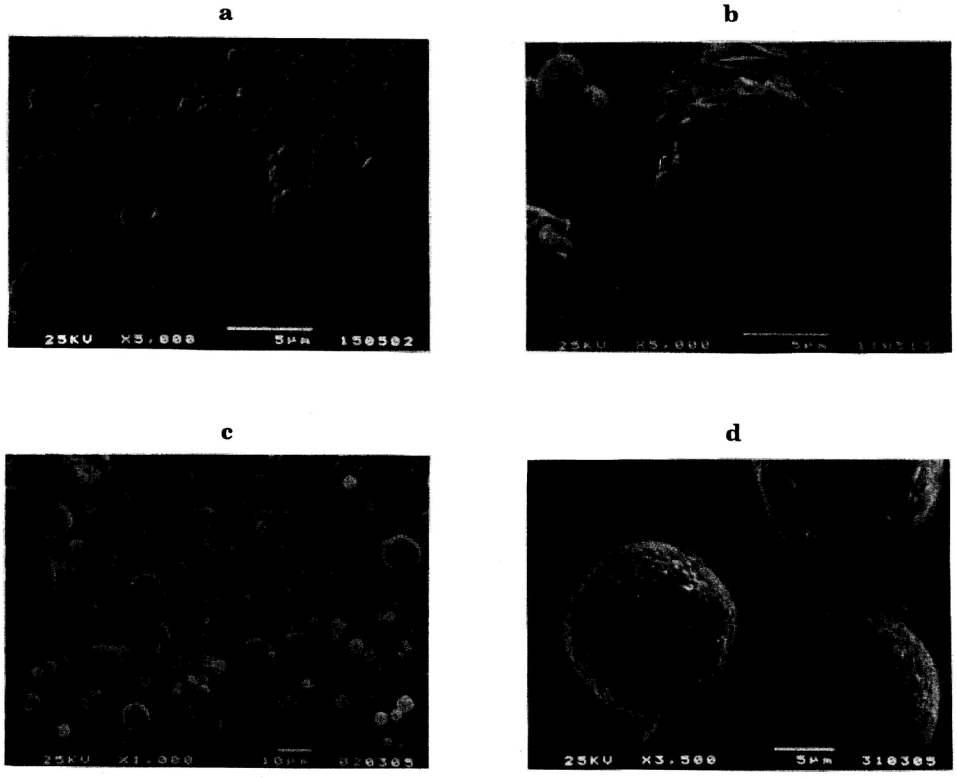

Figure 4. Scanning electron micrographs of (a) $AlPO_4$-20 (sample 1), (b) $AlPO_4$-20(Mn) (sample 3), (c) SAPO-20 (sample 4) and (d) SAPO-20(Mn) (sample 8) crystallized;
a,c,d) under conditions in Table I, b) aged 2 days at 20 °C and then crystallized in 16 hours at 160 °C

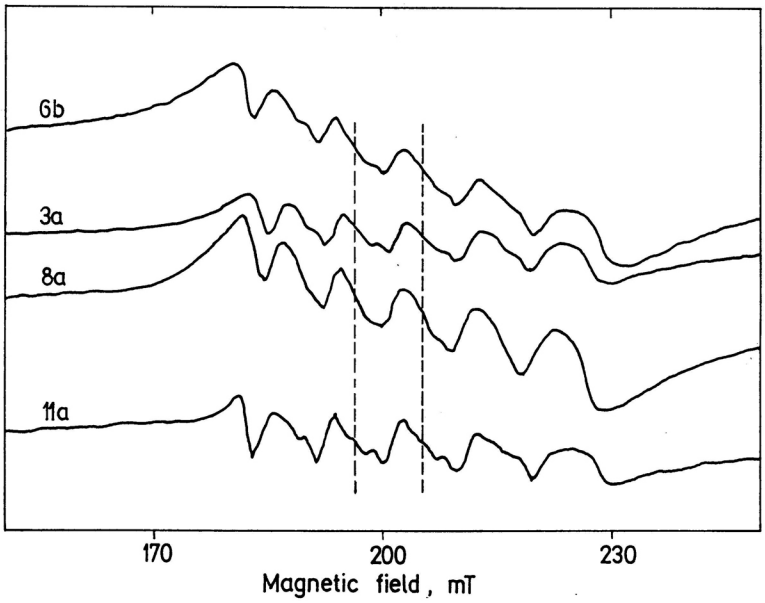

Figure 5. EPR spectra recorded at -133 °C, of some samples (Table IV);
(sample 6b) SAPO-20 impregnated with solution of $MnSO_4$
(sample 3a) $AlPO_4$-20(Mn)
(sample 8a) SAPO-20(Mn)
(sample 11a) aluminophosphate gel containing Mn

TABLE V

Observed bands position in the diffuse reflectance spectra of some $AlPO_4$-20(Mn) and SAPO-20(Mn) samples and of the reference manganese compounds

Sample/No.	Colour	Position of the maximum, nm
gel (see Table I, sample 8)	white powders	365(sh), 406, 419(sh) 442(sh)
$AlPO_4$-20(Mn), sample 3		333(sh), 368(sh), 406, 418(sh), 442(sh), 530(sh)
SAPO-20(Mn), sample 8		339(sh), 367(sh) 406, 419(sh) 439(sh) 510(sh)
SAPO-20(Mn), sample 9		335(sh) 365(sh) 406, 419(sh), 440(sh), 560(sh)
$MnCl_2 \cdot 4H_2O$	pale pink	330, 351(sh), 395, 413(sh), 437(sh), 531(sh)
$[(C_2H_5)_4N]_2\ MnCl_4$	pale yellow-green	350, 369(sh), 425, 440, 462(sh)

sh = shoulder

CONCLUSIONS

Aluminophosphates and silicoaluminophosphates having the sodalite structure have been synthesized: $AlPO_4$-20, $AlPO_4$-20(Mn), SAPO-20, and SAPO-20(Mn). The chemical modification of $AlPO_4$-20 materials with Mn and Si influences the changes in the cubic unit cell dimensions and also affects the thermal stability: $AlPO_4$-20 > SAPO-20 > $AlPO_4$-20(Mn), SAPO-20(Mn). The oxide composition of SAPO-20 affects the number and the temperature range of thermal effects belonging to TMA decomposition and also affects the thermal stability of the sodalite structure. As compared

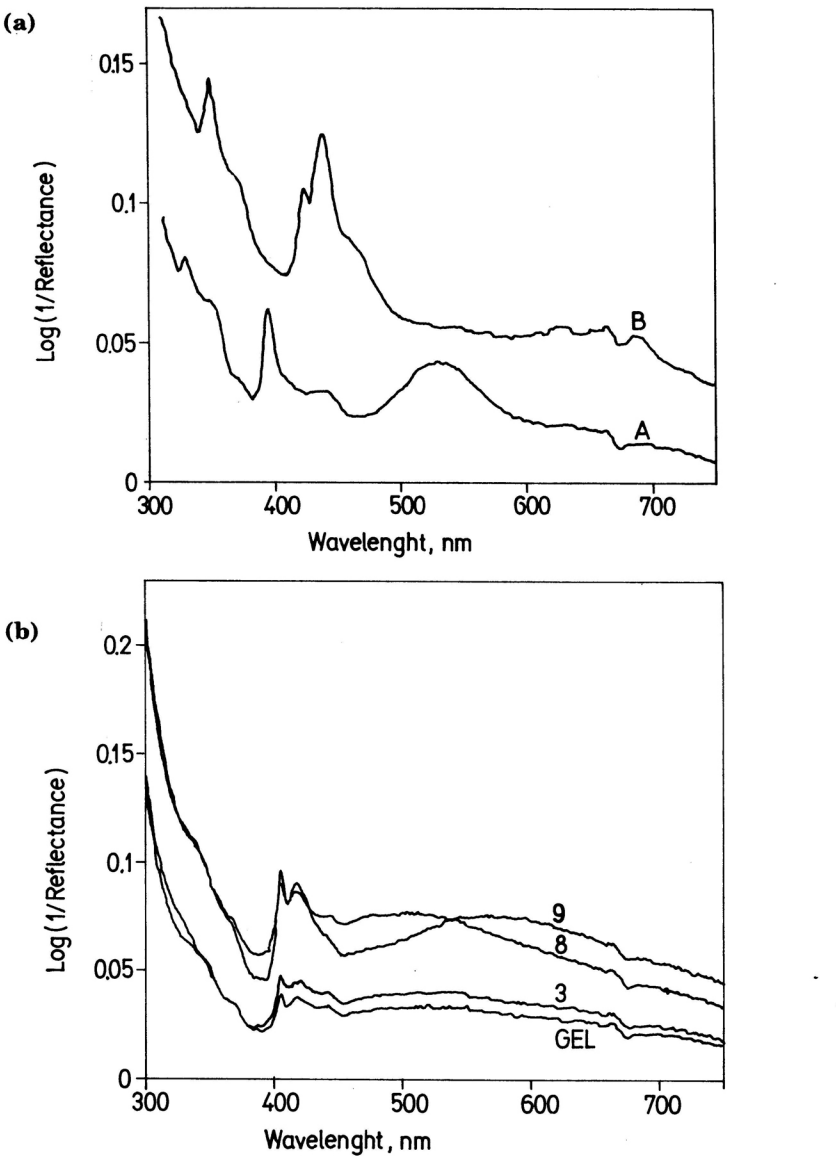

Figure 6. Diffuse reflectance spectra of (a) reference manganese species (A, $MnCl_2.4H_2O$; B, $[(C_2H_5)_4N]_2MnCl_4$) and (b) amorphous material containing Mn, as-synthesized $AlPO_4$-20(Mn) (sample 3, Table I) and SAPO-20(Mn) (samples 8 and 9, Table I).

to the SAPO-20 materials, the thermal effects in all SAPO-20(Mn) are sharper, and their temperature range is narrower. All of the prepared SAPO-20 and SAPO-20(Mn) materials have a TMA/cage ratio lower than one and are dark coloured. The EPR and

DRS data show the presence of octahedrally coordinated non-framework Mn and the presence of these Mn-entities can be the reason for the relatively large change in the unit cell volume and the thermal properties of $AlPO_4$-20(Mn) and SAPO-20(Mn) materials. However, the unit cell parameter data and the thermal behaviour of the samples are not conclusive enough to state that none of the Mn is incorporated into the framework of $AlPO_4$-20(Mn) and SAPO-20(Mn).

Acknowledgement. – We thank Msc. Roman Gabrovšek for TG/DSC measurements.

REFERENCES

1. S. T. Wilson, B. M. Lok, and E. M. Flanigen, *U.S. Patent* 4 310 440 (1982); S. T. Wilson, B. M. Lok, C. A. Messina, T. R. Cannan, and E. M. Flanigen, *J. Amer. Chem. Soc.* **104** (1982) 1146.
2. B. M. Lok, C. A. Messina, R. L. Patton, T. T. Gajek, T. R. Cannan, and E. M. Flanigen, *U.S. Patent* 4 440 871 (1984); *J. Amer. Chem. Soc.* **106** (1984) 6092.
3. E. M. Flanigen, B. M. Lok, R. L. Patton, and S. T. Wilson, *Pure Appl. Chem.* **58** (1986) 1351.
4. W. M. Meier and D. H. Olson, *Atlas of Zeolite Structure Types*, Butterworths, London, 1987, p. 128.
5. H. Weyda and H. Lechert, *Zeolites: Facts, Figures, Future*, Jacobs and R. A. van Santen (Eds.), Elsevier, Amsterdam, 1989, p. 169.
6. D. Hasha, L. S. Saldarriaga, C. Saldarriaga, P. E. Hathaway, D. F. Cox, and M. E. Davis, *J. Amer. Chem. Soc.* **110** (1988) 2127.
7. B. M. Lok, B. K. Marcus, and E. M. Flanigen, *E. Patent Appl.* 161 490 (1985).
8. H. Pines and W. O. Haag, *J. Amer. Chem. Soc.* **82** (1960) 2471.
9. *Powder Diffraction File-Inorganic Phases* (Search Manual), International Center for Diffraction Data, Swarthmore, 1986.
10. B. M. Lok, T. R. Cannan, and C. A. Messina, *Zeolites* **3** (1983) 282.
11. M. Mertens, J. A. Martens, P. J. Grobet, and P. A. Jacobs, *Guidlines for Mastering the Properties of Molecular Sieves*, D. Barthomeuf, E. G. Derouane, and W. Holderich (Eds.), Plenum Press, New York, 1990, p.1.
12. P. E. Werner, *Arkiv Kemi* **31** (1969) 513.
13. J. M. Stewart, P. A. Machin, C. W. Dickinson, H. L. Ammon, H. Heck, and H. Flack, *XRAY-76, X-ray System of Crystallographic Programs,* Computer Science Center, University of Maryland, College Park, Maryland, U. S. A., 1976.
14. D. R. Pyke, P. Whitney, and H. Houghton, *Appl. Catal.* **18** (1985) 173.
15. E. M. Flanigen, R. L. Patton, and S. T. Wilson, *Innovation in Zeolite Materials Science*, P. J. Grobet, W. J. Mortier, E. F. Vansant, and G. Schulz-Ekloff (Eds.), Elsevier, Amsterdam, 1988, p. 13.
16. D. M. Bibby and M. P. Dale, *Nature* **317** (1985) 157.
17. E. M. Flanigen, H. Khatami, and H. A. Szymanski, *Molecular Sieve Zeolites-I*, Am. Chem. Soc., Washington, D. C., 1971, p. 201.
18. *The Aldrich Library of FTIR Spectra*, 1st ed., vol. 1, 1985, 378B.
19. S. P. Zdhanov and N. N. Samulevich, in *Proc. 5st Int. Zeol. Conf.*, L. C. V. Rees, Ed., Heyden, London, 1980, p. 75.
20. V. Strauch and M. Schara, *Internal Report IJS/DP/* 5604, 1989.
21. R. L. Carlin, *Magnetochemistry*, Springer Verlag, Berlin, **64** (1986) 274.
22. R. L. Carlin, *Transition Metal Chemistry,* Marcel Dekker Inc., New York, 1966, vol. 3, p. 170.
23. J. Kliava and J. Purans, *J. Magn. Reson.* **40** (1980) 33.
24. J. Kliava, *Physica Statui Solidi B* **134** (1986) 411.
25. D. Goldfarb, *Zeolites* **9** (1989) 509.
26. N. S. Gill and F. B. Taylor, *Inorg. Syntheses*, S. Y. Tyree, Jr. (Ed.), McGraw Hill, New York, 1967, vol. 9, p. 1365.
27. F. A. Cotton, D. M. L. Goodgame, and M. Goodgame, *J. Amer. Chem. Soc.* **84** (1962) 167.
28. J. J. Foster and N. S. Gill, *J. Chem. Soc. (A)* (1969) 2625.

POVZETEK

Vpliv mangana in silicija na nekatere fizikalno-kemijske lastnosti alumofosfatov s sodalitno strukturo

J. Batista, V. Kaučič in S. Hočevar

Sintetizirali smo alumofosfatne in silikoalumofosfatne materiale sodalitnega strukturnega tipa, ki vsebujejo mangan. Izvedli smo primerjalno študijo lastnosti $AlPO_4$-20, $AlPO_4$-20(Mn), SAPO-20, SAPO-20(Mn), z rentgensko praškovno difrakcijsko analizo, vrstično elektronsko mikroskopijo, EDAX-mikro analizo, kemično in termično analizo, IR, EPR in z DR spektroskopsko analizo. Kemična modifikacija $AlPO_4$-20 z manganom in silicijem vpliva na spremembe parametrov kubične osnovne celice in na termične lastnosti materialov. EPR in DR spektroskopske meritve sintetiziranih $AlPO_4$-20(Mn) in SAPO-20(Mn) materialov kažejo oktaedrično koordinirani mangan, ki ni vgrajen v alumofosfatno oziroma silikoalumofosfatno rešetko. Parametri osnovnih celic in termične lastnosti teh vzorcev pa ne omogačajo nedvoumnih zaključkov o lokaciji Mn.